



Automotive Science and Engineering

Journal Homepage: ase.iust.ac.ir

ISSN: 2008-9899



Effect of Input Heat of Resistance Spot Welding (RSW) Process on the Mechanical Behavior of Welded Joint of SS-316L Steel

Moslem Mohammadi Soleymani¹, Benyamin Sohrabinejad², AliAkbar Majidi Jirandehi^{3*}

¹Mechanical Engineering Department, Payame Noor University, Tehran, Iran

²M. Sc in Mechanical Engineering, Khwarazmi Science and Technology University Qeshm, Iran

³Mechanical Engineering Department, Payame Noor University, Tehran, Iran

ARTICLE INFO

Article history:

Received : 14 Feb 2024

Accepted: 19 May 2024

Published: 26 Jun 2024

Keywords:

316 stainless steel

Resistance spot welding

Input heat

Mechanical behavior

ABSTRACT

In the automobile sector, stainless steel and resistance spot welding (RSW) are often used. In this work, RSW was used to join five samples of 316L stainless steel joints at currents of 15, 20, 25, 30, and 35 kA while the heat input parameters varied. The welded joints' microstructure, hardness, and mechanical properties were examined and evaluated. The base metal, heat-affected zone (HAZ), and weld areas' microstructures were all examined using optical microscopy. The mechanical characteristics of the joints were assessed using room-temperature tensile-shear testing and hardness testing. The microstructure findings revealed ferrite in many weld regions and an austenitic structure overall. In the samples with welding currents of 15, 20, 25, 30, and 35 kA, the average hardness of the weld zone was 329, 258, 251, 238, and 235 Vickers, in that order. The hardness of the weld zone exhibited an inverse connection with the welding current, as an increase in welding current resulted in a drop in the resistance spot welded area's hardness. Furthermore, when heat input increased, the hardness of the HAZ reduced and increased relative to the 316L steel. The joint strength of the RSW increased with increasing welding current, as demonstrated by the tensile-shear test results for all five welded samples with varying currents. As a result, the samples with 30 and 35 kA currents failed at the weld with a force greater than 3 kN, while the other samples with lower welding currents had a failure force of less than 2 kN.

1.Introduction

One of the most popular steels on the market is austenitic stainless steel, which is often used in high-temperature, aqueous, corrosion-resistant

applications. These steels are highly formable and weldable, and they often show a notable increase in length under tensile stress in addition to their great flexibility and toughness. The oil and gas, power generating, automobile, and

*Corresponding Author

Email: Aliakbar.majidi@PNU.ac.ir

<http://doi.org/10.22068/ase.2024.676>

Effect of Input Heat of Resistance Spot Welding (RSW) Process on the Mechanical Behavior of Welded Joint of SS-316L Steel

refinery sectors all make extensive use of this steel. This steel's high chromium content accounts for its resistance to oxidation at high temperatures [1-3]. The impact of heat input during the welding process on the microstructure and mechanical properties of stainless steel joints has been extensively studied; however, the effects of heat input during resistance spot welding (RSW) on the mechanical properties of stainless steel welded joints have received relatively little attention.

Resistance spot welding is a technique that involves pressing two copper electrodes against one another and sandwiching two metal sheets in between. A closed circuit is established, and an electric current begins to flow through the sheets when the electrodes come into contact with them. This causes the material to melt because of the Joule effect, in which the current's passage generates heat. The resistance is highest at the interface between the sheets, where the weld pool begins. This is because copper has a low resistance, and the materials between them typically have twice the resistance. This results in the highest resistance being at the interface between the sheets. Resistance spot welding is the most common method for joining sheets due to its high efficiency and suitability for automated production lines and mass production, especially in automotive bodywork [4].

Resistance spot welding was serendipitously developed by Elihu Thomson while conducting other experiments, which ultimately led to the combination of two copper wires (in 1885). Registered inventions for resistance welding date back to 1900. A few years later, he merged his company with the well-known General Electric company of Thomas Edison. The automobile industry began using this technology in 1930, and both production and maintenance efficiency increased [5].

The most common technique for welding thin metal sheets is RSW. High-speed heat production and minimizing heat loss to the base metal via conduction with the cooling electrodes are two fundamentals of the RSW process. According to reports, the rate of cooling during RSW of steels ranges between about 3000°C per second for sheets that are 2 mm thick and 8000°C per second

for sheets that are 0.8 mm thick [6, 7]. The small volume of the molten zone, the short process time, and the presence of water-cooled copper electrodes are the causes of this fast cooling rate [8, 9]. The metallurgical problems of softening and decreased hardness in the heat-affected zone (HAZ) accompany this fast rate of cooling. Thus, an examination of the metallurgical behavior and mechanical properties of stainless-steel welds is required, given the utilization of RSW and the use of stainless steel in the automobile and home appliance sectors.

As shown in Figures 1 and 2, the time cycle of a spot weld is divided into four primary phases that correlate to the total amount of time needed for the spot welding process.

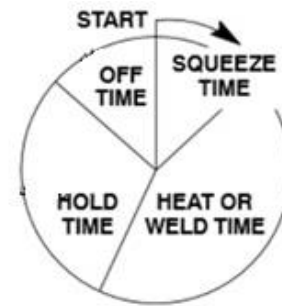


Figure 1: Time cycle of spot weld [5]

The compression time occurs before the welding time (corresponding to period 1); during this period, no current is generated, as the primary objective is to allow the electrodes to reach the required compressive force for welding, but the welding characteristics are not affected. If the compression time is not properly adjusted, ejection of the molten metal from the weld or an explosion between the electrode and the workpiece is possible.

During the hold time (period 3), the current through the electrode/workpiece is stopped, and the primary objective is to cool the weld (using the cooling system present within the electrodes) so that it has sufficient strength. Higher thicknesses require a longer hold time to ensure that the weld is adequately cooled. A shorter hold time is used for materials with a tendency towards brittleness.

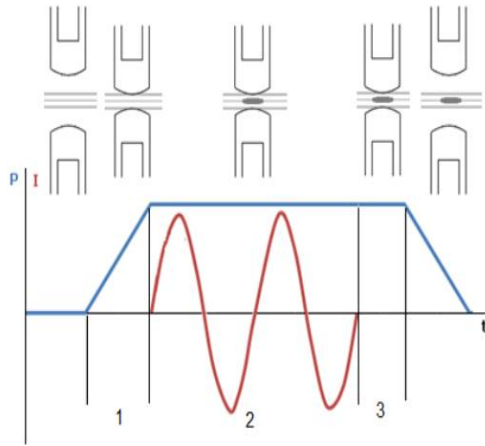


Figure 2: Welding cycles

The largest portion of the time cycle is the welding time, which corresponds to the period when current is introduced into the material. The welding time (period 2) has a direct effect on the dimensions of the workpiece; if it is increased, the heat input increases and the amount of molten material also increases, resulting in larger weld nuggets. Increasing the welding time can lead to problems such as faster electrode wear (due to the temperatures generated on its surface) and potentially deeper indentations on the workpiece, but for materials with a tendency towards brittleness or hardening, longer welding time results in a longer cooling time, which is beneficial to prevent crack formation. The welding time is typically measured in multiple cycles, but it can be measured in the range of a few milliseconds. One cycle corresponds to 20 milliseconds at a power frequency of 50 Hz.

The heat generated is directly dependent on three factors: the current intensity, the resistance of the workpiece, and the duration of current flow (welding time), which is calculated as follows [5]:

$$Q = RI^2t \quad (1)$$

Where $Q[J]$ is the generated heat, $I[A]$ denotes the current intensity, $R[\Omega]$ implies the workpiece resistance, and $t[s]$ is the welding time. The total generated heat is not entirely used for melting the material, and a portion of it is transferred to the surrounding environment and the electrodes. The

only factors that regulate the heat produced are the melting time and the current intensity since the workpiece resistance is not modifiable and is entirely dependent on the melted materials [5].

In their investigation of the connection between the heat input and the austenite grain size, Saumya et al. [10] discovered that the peak temperature in the welding thermal cycle—which is linked to the heat input—controls the austenite grain size at the beginning.

Mechanical and Corrosion Properties of Resistance Spot Welded 316 Stainless Steel Joints, focusing on the welding current (10, 15, and 18 kA) has been checked [11]. More focus should be placed on how welding conditions, particularly the welding heat input, affect the mechanical properties of the HAZ. Lee et al. [12] found that applying a high welding heat input reduces the impact toughness of the HAZ.

A smaller grain size may result in better hardness, according to research conducted by Spanos et al. [13]. Furthermore, hardness reduced when austenite grain size increased, according to Mohanty et al. [14]. Moreover, Morto et al. [15] demonstrated a strong correlation between the austenite grain size and the martensite strength in the HAZ. Nevertheless, a few studies, particularly for high-strength steels, have thoroughly examined the connection between the welding heat input, austenite grain size, hardness, and impact toughness of the HAZ.

In addition to the initial grain size of austenite, the microstructure, which is defined by the phase transition during welding, has a significant impact on the characteristics of the HAZ. According to Dehwa et al. [16], the microstructure of the weld joints is significantly influenced by the welding heat input. As the weakest area of the weld metal, greater focus should be placed on how the welding heat input affects the HAZ's characteristics.

The impact of impact toughness, a crucial component in joint properties, was not addressed in Yun et al.'s [17] discussion of the changes in the microstructure and hardness of the HAZ with welding heat input. Instead, they proposed a microstructure/hardness diagram of the HAZ as a welding process guide. Using a model of

Effect of Input Heat of Resistance Spot Welding (RSW) Process on the Mechanical Behavior of Welded Joint of SS-316L Steel

microstructural development, Bahadessia et al. [18] suggested that the cooling rate governs the different transformation products. Influence of processing conditions on the tensile strength and failure pattern of resistance spot welded SS 316L sheet joint was studied [19].

The impact of welding heat input on the coarse grains in the HAZ was investigated by Chang et al. [20]. They discovered that the impact toughness of the coarse grains in the HAZ diminishes as the welding heat input rises from 30 kJ/cm to 100 kJ/cm, transforming the self-tempered martensite and bainite in the HAZ into bainite and ferrite. Similar researches in recent years can be mentioned by Mohammed et al. [21], Mezher et al. [22], and Bhoyar et al. [23].

The present investigation aimed to examine the impact of the heat input during the RSW process on the mechanical properties of the welded 316L stainless steel joints. An alternating current RSW equipment with a programmable controller was used for this purpose. The welding current (15, 20, 25, 30, and 35) kA was employed, and the values of hold time, welding time, electrode hold time after the current cut-off, and electrode force were all regulated. The welded joints' microstructure, hardness, and tensile-shear tests under various heat inputs were then examined and evaluated.

1. Materials and Methods

The 316L stainless steel sheets with a thickness of 1 mm were selected for this study. The sheets were prepared according to Figure 3. Welding was performed using a 100 kVA fixed spot weld machine with the ability to adjust all the variables of spot welding. An AC resistance welding machine and class 2 conical-shaped electrodes with a 45-degree angle and 8 mm diameter were used. The values of hold time, welding time, electrode hold time after current cut-off, and electrode force used in this study are presented in Table 1. The welding current was increased from 15 to 35 kA.

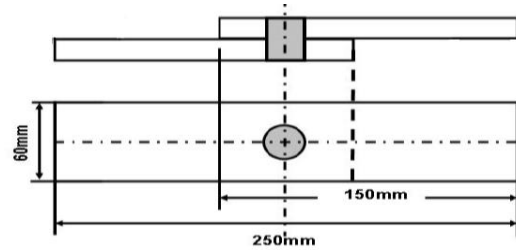


Figure 3: Spot weld joint plan of 316L stainless steel.

Table 1: Resistance spot welding parameters of 316L steel joint.

| current (kA) | Electrode force (kN) | Electrode hold time after current cut-off (s) | Welding time (s) | Hold time (s) | Heat $Q=RI^2t$ |
|-----------------|-------------------------|---|---------------------|---------------------|-------------------|
| 15 | 5 | 0.7 | 1.1 | 5.2 | 247.5 |
| 20 | 5 | 0.8 | 0.9 | 4.7 | 360 |
| 25 | 5 | 0.9 | 0.7 | 4.2 | 437.5 |
| 30 | 5 | 1 | 0.5 | 3.7 | 450 |
| 35 | 5 | 1.1 | 0.3 | 3.2 | 367.5 |

To investigate the macrostructure and microstructure of the base metal, HAZ, and weld in the RSW joints of 316L stainless steel, the sample preparation for macrostructure was performed according to the ASME SEC IX (2017) standard, and for microstructure, it was done according to the ASTM E3:11 standard. The etching solution used was 2% nital and Glyceregia, selected according to the requirements of the ASTM E407:07 standard.

The microstructure of the weld regions, including the base metal, weld metal, and HAZ, were prepared by grinding with 80 to 2000 grit sandpapers, followed by polishing with Al_2O_3 powder. Finally, they were etched using 2% nital and Glyceregia solutions and examined using an optical microscope of Radical RMM2 model.

Figure 4 depicts the 316L steel base metal's microstructure when examined under an optical microscope. The totally austenitic structure of the

316L steel base metal with twinning areas is evident. Some grains have twin structures that are the result of the twin nuclei growing during the annealing process, which occurred during the plastic deformation stage. Since there are no discernible carbide phases or secondary precipitates in the austenitic matrix, the annealing procedure seems to be effective.

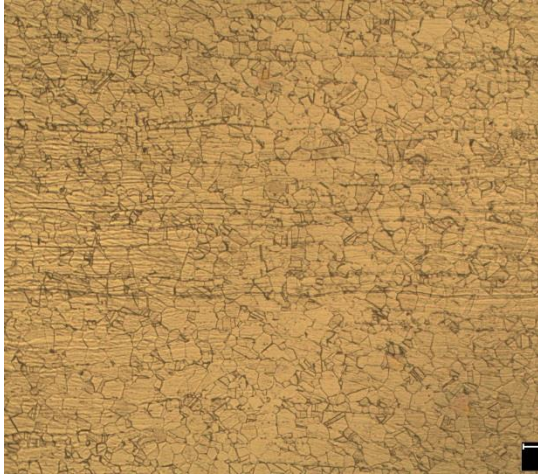


Figure 4: Austenitic microstructure of 316L stainless steel.

Table 2 presents the outcomes of the quantometric examination of the joint's base metal that was carried out utilizing the quantometric approach. The possible phases of the microstructure are predicted in this research using the Schaeffler diagram (Figure 5). Equations 2 and 3 are used to calculate the values of nickel equivalent (Ni_{eq}) and chromium equivalent (Cr_{eq}), respectively. The results are provided in Table 3.

$$Ni_{eq} = \%Ni + 30\%C + 0.5\%Mn \quad (2)$$

$$Cr_{eq} = \%Cr + \%Mo + 1.5\%Si + 0.5\%Nb + 2\%Ti \quad (3)$$

According to the plotted points in Figure 5, according to the calculated values of nickel equivalent (Ni_{eq}) and chromium equivalent (Cr_{eq}), the microstructural phases of the base metal of the joint fall within the A+F region. The expected weld microstructure consists of an austenitic matrix with a small amount of delta ferrite, less than 10% ferrite. For the RSW joint of 316L stainless steel, mechanical tests, including

hardness measurements in the BM, WM, and HAZ regions, as well as tensile-shear tests on the welded sheet samples, were conducted.

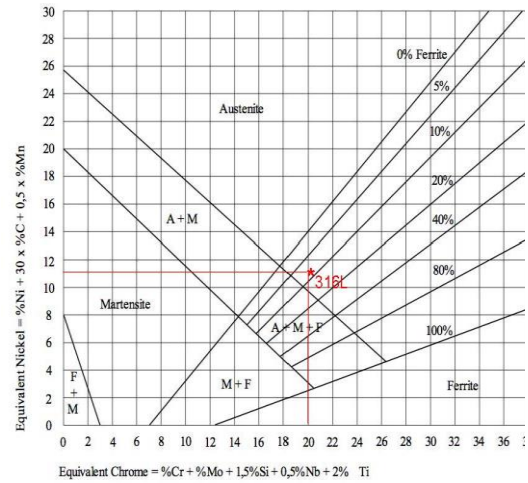


Figure 5: Schaeffler diagram used to predict base and weld metal structure components

In order to investigate the hardness variations in the different regions of the 316L stainless steel RSW joint, the hardness was measured from the weld spot of the samples using an INNOVATEST NOVA 240 Vickers hardness tester with a load of HV0.3 (2.942 N) according to the standard (ISO 6507-1:2018). The tensile-shear test was conducted at room temperature to compare the strength of the weld spots in the samples. The tensile-shear test samples were tested according to the standard ANSI/AWS/SAE D8.9-97 [24]. Two tensile-shear test samples were considered for each joint.

Table 2: Chemical composition of base metal 316L (by weight percentage).

| Element | weight percentage |
|---------|-------------------|
| C | 0.01 |
| Mn | 1.01 |
| Si | 0.51 |
| P | 0.041 |

| Element | weight percentage |
|---------|-------------------|
| S | 0.004 |
| Cr | 17.21 |
| Mo | 2.03 |
| Ni | 10.18 |
| Ti | 0.003 |
| Nb | 0.006 |

Table 3: Equivalent values of nickel and chromium for the joint base metal 316L.

| Cr _{eq} | Ni _{eq} |
|------------------|------------------|
| 20.01 | 10.98 |

3. Results and Discussion

Results of the hardness tests conducted on the various areas of the welded joint, the tensile-shear test conducted on samples with varying welding heat inputs, and the macro and microstructure results of the RSW joint of 316L stainless steel are reported.

3.1 Weld Spot Macro Structure

Figure 7 displays the macro structure of 316L stainless steel RSW at welding currents of 15, 20, 25, 30, and 35 kA, highlighting the various weld areas. The heat produced during welding causes the base metal to remelt in the fusion zone, where it solidifies into a structure with columnar grains. An optical microscope was used to determine the weld nugget diameter, as shown in Figure 7.

The average weld nugget diameter was computed and presented in Table 4. According to the average weld nugget diameter calculation, samples with welding currents of 15 kA and 35

kA had the smallest and largest weld nugget diameters, respectively. The results indicate that an increase in welding current causes an increase in weld nugget diameter. However, as Figure 7(d) illustrates, the sample that used a 25-kA current has a defective cavity in the center of the weld that is 476 μm deep, and the weld nugget dimensions are bigger than those of the other samples. One of the factors that may help manage the mechanical properties of RSW is the increase in joint area that results from increasing the weld nugget diameter [25, 26].

Table 4: Calculation of the average diameter of 316L steel welding nugget.

| Current (kA) | Large diameter (μm) | Small diameter (μm) | Average diameter (μm) |
|--------------|----------------------------------|----------------------------------|------------------------------------|
| 15 | 1180.07 | 846.07 | 1013.07 |
| 20 | 1205.19 | 824.19 | 1014.69 |
| 25 | 1708.75 | 1018.11 | 1394.93 |
| 30 | 1693.73 | 843.44 | 1268.59 |
| 35 | 1711.75 | 850.52 | 1281.14 |

3.2 Microstructure of Different Resistance Spot Welding Zones of 316L Steel

Figure 8 depicts the microstructure of the various areas in the 316L stainless steel RSW observed under an optical microscope. The area between the base metal and the HAZ of 316 steel may be observed to have an austenitic microstructure in the optical microscope images of the HAZ depicted in Figures 8(a) and 8(b).

In the fusion line area, there is an austenitic structure with delta ferrite islands. The microstructure of the HAZ shows the precipitation of delta ferrite in an austenitic matrix as one approaches the weld interface. During cooling to room temperature, the structure enters a two-phase austenite + ferrite region, and most of the delta ferrite formed during solidification becomes unstable and transforms back to austenite.

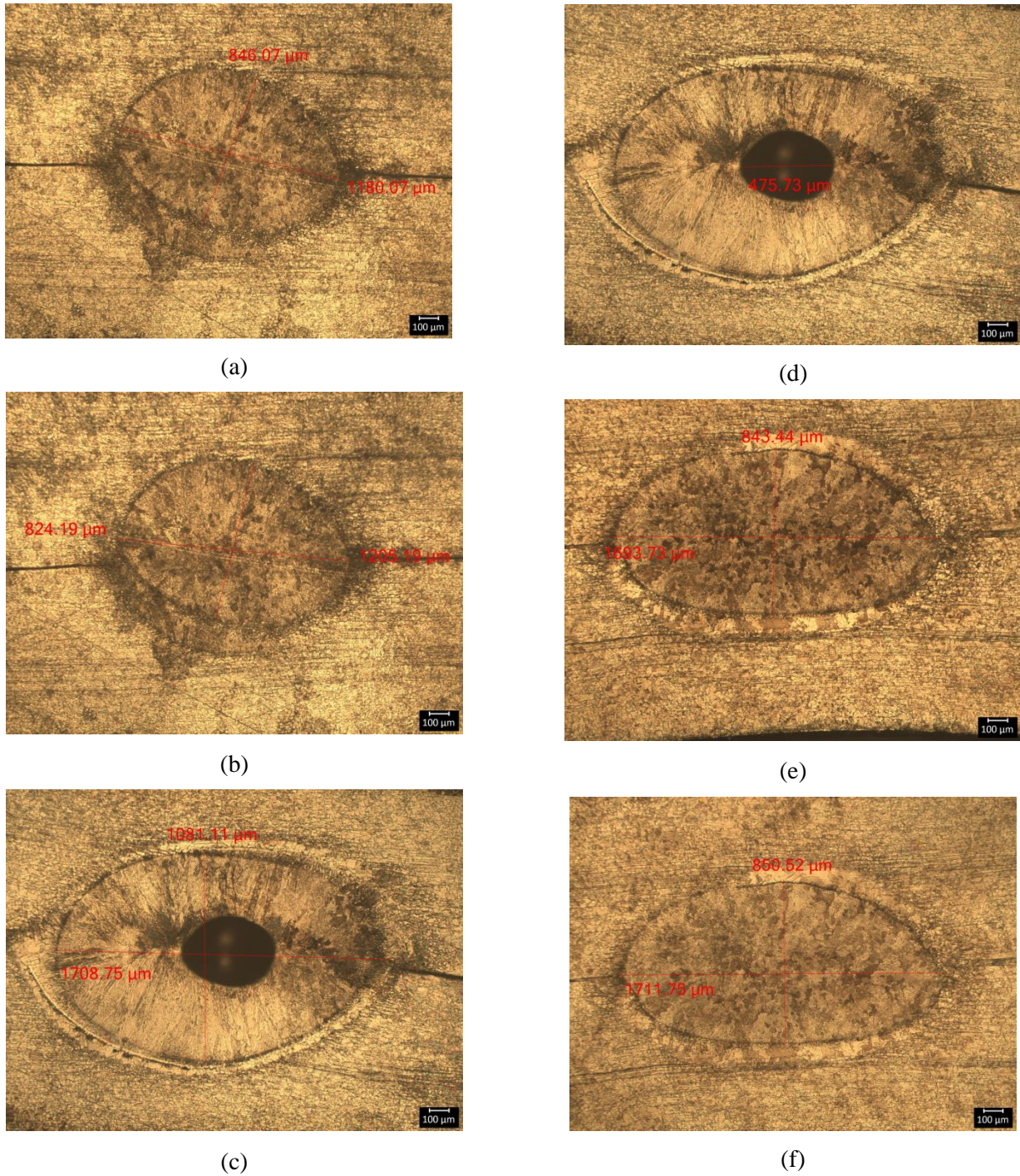


Figure 7: Macro images of the structure of 316L steel welding nugget with different currents. a) Welding nugget of the 15 kA sample, b) Welding nugget of the 20 kA sample, c) Welding nugget of the 25 kA sample, d) Cavity created in the 25 kA sample, e) Welding nugget of the 30 kA sample, f) Welding nugget of the 35 kA sample.

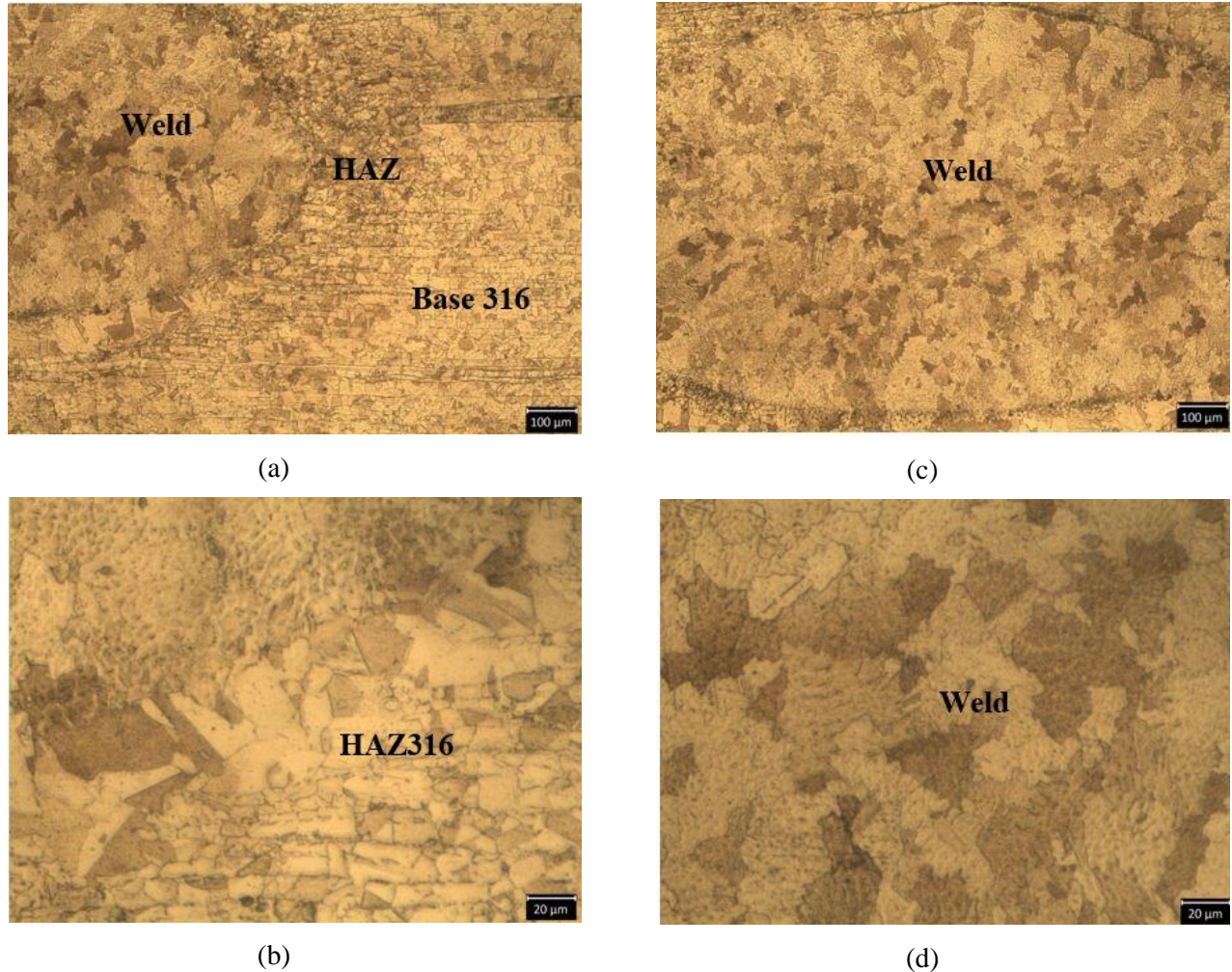


Figure 8: Microstructure of different zones of the 316L steel spot weld.

a) 316L steel interface with HAZ, b) HAZ, c) Weld spot, d) Weld spot.

The dendritic cores, which solidified first, remain as delta ferrite rich in chromium up to room temperature, and this microstructure continues up to the weld interface.

As observed in Figure 8(a) and 8(b), there is no significant change in the grain size when moving from the base metal towards the weld fusion line up to the vicinity of the fusion line. It is at the region immediately adjacent to the fusion line where grain growth has occurred. The rise in temperature that occurs during welding is the cause of the grain formation in these locations. The temperature of these surrounding areas increases as a result of the substantial heat transfer that occurs during the welding process

from the weld zone. The surrounding regions take some time to cool down because of their substantial thermal capacity and the limited thermal conductivity of the austenite phase. As a result, these regions remain at elevated temperatures for a certain duration, and this leads to the natural consequence of grain growth in the vicinity of the weld fusion line.

Figures 8(c) and 8(d) indicate the weld microstructure in the RSW of the 316L stainless steel used in this study. The optical micrograph in Figure 8(c) reveals a weld microstructure consisting of austenite with a distribution of delta ferrite phase within the austenite matrix. The microstructure is austenitic, as expected,

comprised of approximately coaxial grains. This single-phase austenitic (Type A) solidification mode is attributed to the segregation of alloying elements and impurities during the solidification process.

As observed in Figure 8, the weld microstructure has solidified in an austenitic structure with delta ferrite islands, which is consistent with the chemical composition and the calculated chromium-to-nickel equivalent ratio presented in Table 3. The ferrite phases are located at the core of the primary ferrite dendrites. The weld metal solidifies initially as delta ferrite along with austenite in the interdendritic regions. After solidification is completed and cooling to room temperature, the structure enters the dual-phase austenite + ferrite region, and the majority of the delta ferrite formed during solidification becomes unstable and transforms into austenite. This results in the final microstructure consisting of an austenitic matrix with delta ferrite islands, as shown in Figure 8(c).

3.3 Hardness Measurement

Vickers hardness measurements were used in the RSW of 316L stainless steel to assess the hardness in the base metal, HAZ, and weld metal regions of the welded connection. Table 5 and Figure 9 provide a comparison of the Vickers hardness test results for the welded samples produced with varying welding currents.

The hardness is a function of the chemical composition, the volume fractions of the microstructural phases formed, and the thermal changes in the base metal and the weld. The 15kA sample has the maximum weld hardness, while the 35kA sample has the lowest, as can be seen in the figure. The HAZ and base metal had lower hardness values than the weld metal in all samples at different welding currents.

The values of 329, 258, 251, 238 and 235 Vickers, respectively, are the average hardness of the weld metal in the samples with welding currents of 15, 20, 25, 30, and 35 kA. The 15 kA sample's weld metal has the maximum hardness, while the 35 kA sample's weld metal has the lowest, as illustrated in Figure 10. The weld

region's hardness reduces as the RSW current increases.

Table 5: Vickers hardness of different spot weld zones in 316L steel joint.

| Sample | 15 kA | 20 kA | 25 kA | 30 kA | 35 kA |
|----------------|-------|-------|-------|-------|-------|
| Point 1 (BM) | 176 | 181 | 193 | 173 | 181 |
| Point 2 (BM) | 180 | 176 | 195 | 174 | 174 |
| Point 3 (HAZ) | 211 | 213 | 229 | 214 | 210 |
| Point 4 (HAZ) | 217 | 222 | 231 | 218 | 204 |
| Point 5 (Weld) | 326 | 262 | 249 | 239 | 233 |
| Point 6 (Weld) | 332 | 255 | 253 | 237 | 238 |
| Point 7 (HAZ) | 229 | 324 | 230 | 216 | 209 |
| Point 8 (HAZ) | 220 | 227 | 233 | 210 | 212 |
| Point 9 (BM) | 187 | 170 | 193 | 174 | 177 |
| Point 10 (BM) | 184 | 173 | 188 | 177 | 180 |

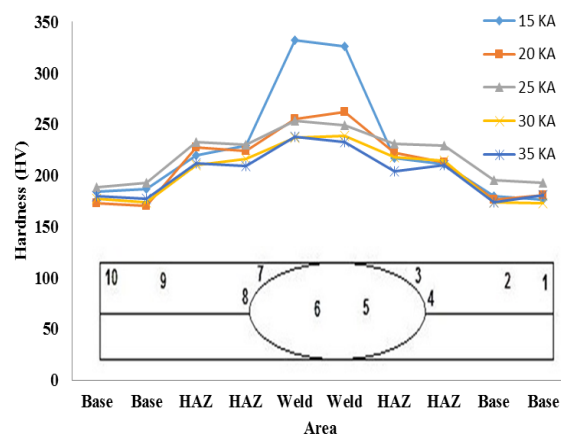


Figure 9: Vickers hardness changes of spot weld of 316L steel in different welding currents.

Effect of Input Heat of Resistance Spot Welding (RSW) Process on the Mechanical Behavior of Welded Joint of SS-316L Steel

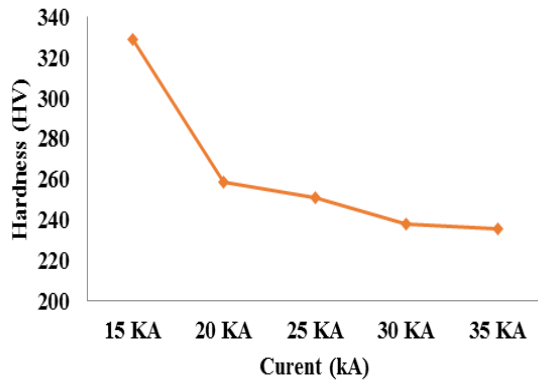


Figure 10: Correlation between welding current and average weld hardness of 316L steel joint.

The increase in heat input during welding is responsible for the reduction in weld hardness because it alters the shape of the weld metal. Increased heat input causes a slower rate of cooling, which prolongs the weld's capacity to remain at higher temperatures. As a consequence, coarser grains are formed, which lowers the hardness [27].

Since chromium carbides are present and welding thermal cycles are performed in this area, the hardness of the 316L steel in the HAZ increased in all five forms of welding currents. Figure 8 demonstrates that the weld metal and the HAZ microstructures showed an equiaxed austenitic structure with ferrite.

Furthermore, an increase in hardness from the base metal to the weld area inside the HAZ was observed as a result of the welding heat input. This may be explained by the grains being coarser from the weld center toward the base metal, as well as by the base metal containing carbides of the alloying elements and intermetallic phases, which can cause the hardness to rise from the weld center toward the base metal.

The diversity of hardness across the weld regions is shown in Table 5, indicating the prevalent heterogeneous microstructure in the different weld zones. Additionally, the average Vickers hardness values for the base metal and the HAZ demonstrate a similar behavior to that of the weld metal in the five different samples. The average HAZ hardness on both sides of the weld

was higher than that of the base metal. The welding heat input reduces the cooling rate of the HAZs, leading to the growth of austenite grains, and consequently, altering the HAZ characteristics, including its hardness [28, 29].

3.4 Tensile-shear test

In order to identify the suitable heat input for the desired mechanical properties of these joints, the tensile-shear test was used to examine the mechanical properties of the resistance spot welded S316L steel joints with various welding currents. Table 6 and Figure 11 illustrate the tensile-shear test results for the welded samples employing five different welding currents. In the tensile test, all the samples failed in the welding area.

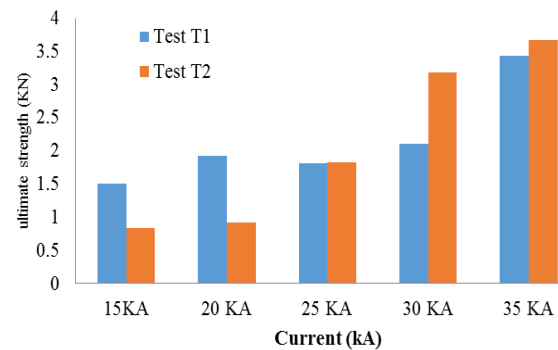


Figure 11: Comparison of fracture force of welded samples with different currents.

According to the tensile-shear test outcomes, the weld strength was lower for the two welded samples with welding currents of 15 kA and 20 kA than for the other samples, where the tensile sample failed at the weld with a force less than 1 kN. However, the failure load of the joint was higher in the samples with welding currents of 30 kA and 35 kA than in the other three samples. This suggests that the weld quality was fully validated in terms of weld soundness and that the defects in the samples with welding currents of 30 kA and 35 kA did not affect the mechanical

properties of the welds. Table 6 and Figure 11 indicate that when the welding current increases from 15 kA to 35 kA, the welded sample's joint strength and failure load rise as well. The sample with the highest joint strength achieved has a welding current of 35 kA.

The mechanical properties of the 316L stainless steel joints welded by RSW are impacted by the change in welding current, according to the analysis of the data from Table 6 and Figure 12.

Table 6: Results of the tensile-shear test.

| Sample | ultimate strength (KN) |
|--------|------------------------|
| 15-T1 | 1.5 |
| 15-T2 | 0.83 |
| 20-T1 | 1.93 |
| 20-T2 | 0.92 |
| 25-T1 | 1.81 |
| 25-T2 | 1.83 |
| 30-T1 | 2.11 |
| 30-T2 | 3.18 |
| 35-T1 | 3.43 |
| 35-T2 | 3.67 |

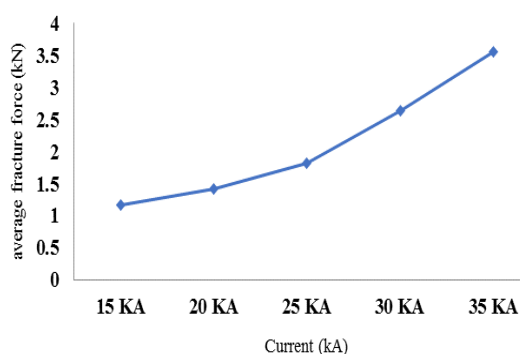


Figure 12: Correlation between welding current and average fracture force of 316L steel joint.

The average fracture strength of the sample with a welding current of 15 kA was 22% lower than that of

the sample with a welding current of 20 kA. On the other hand, the average joint failure load increased by 28% when the welding current was raised from 20 kA to 25 kA. Table 6 additionally demonstrates that, for samples with welding currents of 30 kA and 35 kA, changes in the joint failure load under the same conditions were about 45% and 95% higher, respectively, compared to the sample with a 25-kA welding current. As a result, alterations in the mechanical properties were more than 200% higher than for the sample with a 15-kA welding current. According to Figure 12, the weld fracture load increases in conjunction with an increase in welding current. The weld nugget diameter increases as the welding current increases. This finding is supported by Figure 7 of the weld nugget's macro graphic data. An increase in the joint area can be observed by the weld nugget diameter. An increase in this parameter increases the joint failure load because the weld nugget diameter is the main parameter governing the mechanical properties of RSW [25, 30].

4. Conclusions

Using five different welding currents, the microstructure and mechanical properties of 316L stainless steel RSW joints were examined in this research. The findings were as follows.

- The 316L steel welding joint's base metal microstructure shows evidence of a completely austenitic structure.
- The macro graphic analysis of the sample weld nuggets revealed that an increase in welding current causes the weld nugget diameter to expand.
- Under various welding currents, the microstructure of the 316L steel RSW joint is austenitic and exhibits the distribution of the delta ferrite phase. The investigation of the Schaeffler diagram for spot welds indicates that the microstructure has less than 10% ferrite and is located in the austenite area.
- The hardness of the weld zone and the welding current have an inverse relationship; that is, as the welding current increases, the RSW region's hardness decreases. Furthermore, in comparison to the 316L base metal, the HAZ's hardness rises, and it

decreases with an increase in the welding process's heat input.

- The tensile-shear test results for each of the five welded samples with various welding currents demonstrate that the RSW joint strength increases with a rise in welding current.

References

- [1] H. Shah, Hosseini, M. Shamanian, A. Kermanpur, Characterization of microstructures and mechanical properties of Inconel 617/310 stainless steel dissimilar welds, *Materials characterization*, Vol. 62, No. 4, (2011), pp. 425-431.
- [2] A. Ambroziak, M. Korzeniowski, P. Kustron, Quality control of spot welds—the challenge for automotive industry, *inżynieria produkcji. Wiedza–wizja–programy ramowe*. InPod red. E. Chlebusa, (2006), pp. 359-366.
- [3] A. Ambroziak, M. Korzeniowski, Using Resistance Spot Welding for Joining Aluminium Elements in Automotive Industry, *Archives of Civil and Mechanical Engineering*, Vol. 10, (2010), pp. 5–13.
- [4] Resistance Welding Manual, Rautaruukki Corporation, (2009) pp.1–29.
- [5] A Handbook for Resistance Spot Welding, Miller Welds, (2012), pp. 1–9.
- [6] J. E. Gould, S. P. Khurana, T. Li, Prediction of microstructures when welding automotive advanced high-strength steels, *Welding Journal*, Vol. 85, No. 5, (2006), pp. 111-116.
- [7] Handbook, Welding. "Vol. 4: Materials and applications." Part 2 (1998), pp. 137-140.
- [8] X. Wan, Y. Wang, C. Fang, Welding Defects Occurrence and Their Effects on Weld Quality in Resistance Spot Welding of AHSS Steel, *ISIJ International*, Vol. 54, (2014), pp. 1883–1889.
- [8] B.A. Ogunnaike, W.H. Pay, Processes, dynamics, modeling and control. Oxford University Press, Oxford (1994).
- [9] M. Pouranvari, S. P. H. Marashi, critical review of automotive steels spot welding: process, structure and properties, *Science and Technology of Welding and Joining*, Vol. 18, No. 5, (2013), pp. 361-403.
- [10] M. Shome, Effect of heat-input on austenite grain size in the heat-affected zone of HSLA-100 steel. *Materials Science and Engineering: A*, Vol. 445, (2007), pp. 454-460.
- [11] S.R. Mousavi, M. Esmailzadeh, A.S. Hammood, Microstructure, Mechanical and Corrosion Properties of Resistance Spot Welded 316 Stainless Steel Joints: The Effect of Welding Current, *Journal of Manufacturing Innovations*, Vol. 1, No. 1, (2023), pp.52-68.
- [12] Y. Li., D. N. Crowther, M. J. W. Green, P. S. Mitchell, T. N. Baker, The effect of vanadium and niobium on the properties and microstructure of the intercritically reheated coarse grained heat affected zone in low carbon microalloyed steels. *Iron Steel. ISIJ international*, Vol. 41, No. 1, (2001), pp.46–55.
- [13] G. D. W. Spanos, Moon, R. W. Fonda, E. S. K. Menon, and A. G. Fox, Microstructural, compositional, and microhardness variations across a gas-metal arc weldment made with an ultralow-carbon consumable, *Metallurgical and materials transactions A*, Vol. 32, (2001), pp. 3043-3054.
- [14] O. N. Mohanty, M. Shome, Continuous cooling transformation diagrams applicable to the heat-affected zone of HSLA-80 and HSLA-100 steels, *Metallurgical and Materials Transactions A*, vol. 37, No. 7, (2006), pp. 2159-2169.
- [15] S. Morito, H. Yoshida, T. Maki, X. Huang. Effect of block size on the strength of lath martensite in low carbon steels, *Materials Science and Engineering: A*, Vol. 438, (2006), pp. 237-240.

- [16] S. K. Dhua, D. Mukerjee, D. S. Sarma, Weldability and microstructural aspects of shielded metal arc welded HSLA-100 steel plates, *ISIJ international*, Vol. 42, No. 3 (2002), pp. 290-298.
- [17] J. C. Ion, K.E. Easterling, M.F. Ashby, A second report on diagrams of microstructure and hardness for heat-affected zones in welds, *Acta Metallurgica*, Vol.32, No. 11, (1984), pp. 1949-1962.
- [18] H.K.D.H. Bhadeshia, L.E. Svensson, B. Greftoft, A model for the development of microstructure in low-alloy steel (Fe-Mn-Si-C) weld deposits, *Acta Metallurgica*, Vol. 33, No. 7, (1985), pp. 1271-1283.
- [19] D.D. Deshmukh, Y. Kharche, Influence of processing conditions on the tensile strength and failure pattern of resistance spot welded SS 316L sheet joint, *International Journal on Interactive Design and Manufacturing (IJIDeM)*, Vol. 1, No. 1, (2023), pp.1-13.
- [20] Y. Q. Zhang, H. Q. Zhang, J.F. Li, W. M. Liu, Effect of heat input on microstructure and toughness of coarse grain heat affected zone in Nb microalloyed HSLA steels, *Journal of Iron and Steel Research International*, Vol. 16, No. 5 (2009), pp. 73-80.
- [21] H.G. Mohammed, T.L. Ginta, M. Mustapha, The investigation of microstructure and mechanical properties of resistance spot welded AISI 316L austenitic stainless steel, *Materials Today: Proceedings*, Vol. 46, No. 1, (2021), pp.1640-1644.
- [22] M.T. Mezher, A. Pereira, T. Trzepieciński, J. Acevedo, Artificial Neural Networks and Experimental Analysis of the Resistance Spot Welding Parameters Effect on the Welded Joint Quality of AISI 304, *Materials*, Vol. 17, No. 9, (2024), p.2167.
- [23] D. Bhoyar, N. Mungle, A review of microstructure, mechanical properties, and welding of SS316L, *Recent Advances in Material, Manufacturing, and Machine Learning*, (2024), pp.639-648.
- [24] Recommended Practices for Test Methods and Evaluation the Resistance Spot Welding Behavior of Automotive Sheet Steels, ANSI/AWS/SAE D8.9-97, American Welding Society, Miami, FL, USA, (1997).
- [25] M. Pouranvari, S. P. H. Marashi, critical review of automotive steels spot welding: process, structure and properties, *Science and Technology of Welding And Joining*, Vol. 18, No. 5, (2013), pp. 361-403.
- [26] D.V. Kiran, B. B. A. De, Influence of process variables on weld bead quality in two wire tandem submerged arc welding of HSLA steel. *Journal of Materials Processing Technology*, Vol. 212, (2012), pp. 2041-2045.
- [27] C. D. Lundin, G. Zhou, K. K. Khan, Metallurgical Characterization of the HAZ in A516-70 and Evaluation of Fracture Toughness Specimens, *Welding Research Council Bulletin*, No. 403, Report 1, (1995), pp. 1-88.
- [28] X. L. Wan, K. M. Wu, G. Huang, R. Wei, In situ observations of the formation of fine-grained mixed microstructures of acicular ferrite and bainite in the simulated coarse-grained heated-affected zone. *Steel Res. Int.*, Vol. 85, No. 2, (2014), pp.243-257.
- [29] X. L. Wan, R. Wei, K. M. Wu, Effect of acicular ferrite formation on grain refinement in the coarse-grained region of heat-affected zone, *Materials Characterization*, Vol. 61, No. 7, (2010), pp. 726-731.
- [30] M. Pouranvari, S. P. H. Marashi, D. S. Safanama, Failure mode transition in AHSS resistance spot welds. Part II: Experimental investigation and model validation, *Materials Science and Engineering: A*, Vol. 528, No. 29-30 (2011), pp. 8344-8352.